Journal of
Polymer Materials

Tech Science Press

Doi:10.32604/jpm.2026.074541

ARTICLE

The Valorization of Poplar Leaves Waste for the Extraction of Cellulose Nanocrystals

Dongwei Shao, Hao Sun, Qi Wang, Ping Han, Yiwei Liu, Jiyi Luan, Lin Jia, Qiang He and Bo Cui*

College of Mechanical Engineering, Jiamusi University, Jiamusi, 154007, China

*Corresponding Author: Bo Cui. Email: cuibo@qlu.edu.cn

Received: 13 October 2025; Accepted: 06 January 2026; Published: 03 April 2026

ABSTRACT: The valorization of agricultural waste into high-value nanomaterials is crucial for advancing sustainable biorefineries. This study presents an efficient approach for extracting carboxylated cellulose nanocrystals (CNCs) from poplar leaf waste (PL), an abundant and underutilized biomass. The process involved alkaline treatment and hydrogen peroxide bleaching to purify cellulose (PL-CEL), followed by sequential periodate-chlorite oxidation to produce dicarboxylic cellulose nanocrystals (PL-CNCs). The resulting nanocrystals were comprehensively characterized using compositional analysis, XRD, FTIR, TEM, TGA, and zeta potential measurements. XRD analysis confirmed a high crystallinity index of 82% for PL-CEL, which decreased to 72.2% after oxidation due to the introduction of carboxyl groups. FTIR spectra revealed a prominent peak at 1720 cm^{-1}, confirming successful carboxylation. TEM images showed rod-like nanocrystals with an average length of 271.22 nm and width of 14.68 nm, while conductometric titration indicated a carboxyl content of 1.9 mmol/g. The PL-CNCs exhibited good colloidal stability with a zeta potential of −30.2 mV at pH 7.0. TGA demonstrated moderate thermal stability with enhanced char formation. This work highlights a green and scalable route for converting poplar leaf waste into functional nanocellulose, suitable for applications in composites, adsorption, and sustainable materials. The novelty of this study lies in the pioneering use of poplar leaf waste combined with a sequential periodate-chlorite oxidation to sustainably produce carboxylated CNCs with enhanced functionality.

KEYWORDS: Poplar leaves; sequential oxidation; cellulose nanocrystals; carboxylation; waste valorization

1 Introduction

The global transition toward sustainable economies has intensified the demand for renewable materials to replace petroleum-based products. Among biopolymers, cellulose, characterized by linear chains of β-(1→4)-linked D-glucose units, is the most abundant structural polysaccharide on Earth [1]. Its native structure comprises both highly ordered crystalline regions and disordered amorphous domains (Fig. 1) [2,3]. Through controlled disintegration, cellulose can be converted into nanocellulose-a high-value nanomaterial categorized primarily as cellulose nanocrystals (CNCs) or cellulose nanofibrils (CNFs) [4,5]. These nanomaterials exhibit exceptional properties, including biodegradability, low density, high specific surface area, and superior mechanical strength, making them suitable for advanced applications in composites [6], biomedicine [7], energy storage [8,9], and environmentally friendly packaging [10], tissue engineering [11], smart sensors [12]. The growing market for sustainable nanomaterials underscores the importance of diversifying feedstock sources and optimizing production processes [13–16].

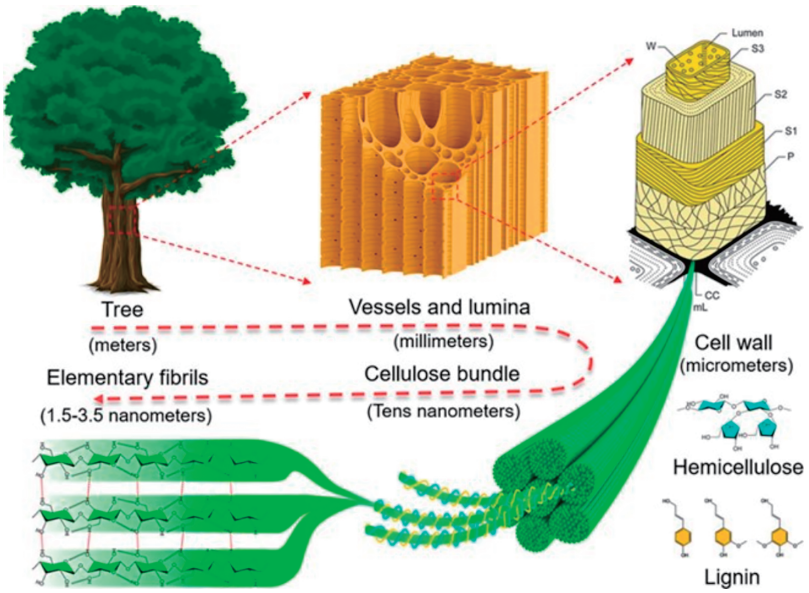

Figure 1: Hierarchical structure and anisotropy of wood, from macroscopic to molecular scale. Reprinted with permission from Chen and Hu (2018) [3]. Copyright © 2018 American Chemical Society

Conventional methods for nanocellulose isolation include mechanical, chemical, and enzymatic approaches, each with inherent limitations. Mechanical techniques such as high-pressure homogenization, ultrasonication, and ball milling often require high energy input and can damage cellulose crystallinity [17–19]. Chemical methods, particularly acid hydrolysis using sulfuric acid, are effective in removing amorphous regions but raise concerns about environmental impact, corrosion, and the need for extensive purification [20]. For instance, sulfuric acid hydrolysis introduces sulfate ester groups, enhancing colloidal stability but potentially reducing thermal stability [21]. Emerging green solvents, such as low-transition-temperature mixtures (e.g., acid-based DES like formic acid/choline), offer a sustainable alternative by acting as multifunctional platforms for simultaneous nanocellulose production and functionalization, reducing energy consumption by over 40% [22–24]. Similarly, TEMPO-mediated oxidation enables efficient carboxylation of cellulose under mild conditions, producing nanocellulose with high colloidal stability and minimal structural degradation [25]. However, these methods often rely on purified wood pulp or specialized feedstocks, which are costly and not always sustainable. In contrast, this study adopts a sequential periodate-chlorite oxidation approach, which selectively converts C2–C3 bonds of glucose units into aldehyde and subsequently carboxyl groups, offering precise control over surface functionality and enhanced hydrothermal stability without requiring harsh acids. This method aligns with green chemistry principles by minimizing chemical waste and enabling efficient conversion under moderate conditions.

Poplar leaves, an abundant agricultural waste, represent a promising and underexplored source of cellulose [26,27]. Existing studies have explored nanocellulose extraction from various leaf sources, such as pineapple leaf fiber, simpor leaf residue, and ginkgo leaves. For instance, patent CN106345426A details a method using TEMPO oxidation or hydrolysis systems to extract nanocellulose from leaves like ginkgo and pine, achieving diameters of 1–100 nm and high adsorption capacity for heavy metal ions. Similarly, microcrystalline cellulose was successfully isolated from *Tephrosia purpurea* leaves via chemical treatment, exhibiting a crystallinity index of 54.56% and a crystalline size of 15.68 nm, with a maximum degradation temperature of 367.63°C [28]. In another study, acid hydrolysis was employed to extract microcrystalline cellulose from *Ocimum tenuiflorum* leaves, yielding a crystallinity index of 68.94% and a crystallite size of

13.38 nm, while the maximum degradation temperature was recorded at 187.83°C [29]. In the work of Fouad et al., microcrystalline cellulose was first isolated from pineapple leaf fibers through a sequence of bleaching, alkali, and acid treatments, and further functionalized into carboxymethyl microcrystalline cellulose via reaction with sodium hydroxide and chloroacetic acid [30]. Microcrystalline cellulose was also extracted from delignified Serte leaf fiber wastes using hydrochloric acid hydrolysis, achieving a crystallinity of 73.5% and a particle size in the range of 30–60 μm [31]. However, these studies face challenges, including variable cellulose content (10%–30% in leaves), complex compositional heterogeneity, and the presence of recalcitrant compounds like lignin and extractives, which necessitate energy-intensive pretreatments [32]. Additionally, many methods yield nanocellulose with inconsistent morphology or insufficient functionality for advanced applications. In contrast, poplar leaves (e.g., from Populus species) offer distinct advantages: higher annual yield from widespread cultivation, consistent cellulose content (approximately 36%, comparable to rice straw), and minimal competition with food or feed sources. Their utilization not only supports waste valorization but also reduces reliance on traditional wood-based feedstocks, offering a low-cost and readily available resource. This study addresses the limitations of prior leaf-based research by employing poplar leaves, which are largely underexplored, and combining alkaline pre-treatment with sequential oxidation to achieve higher purity and functionality.

In this work, cellulose was extracted from poplar leaf waste through alkaline treatment and bleaching, followed by sequential periodate-chlorite oxidation to produce carboxylated cellulose nanocrystals (CNCs). The structural, morphological, and thermal properties of the resulting nanocellulose were characterized using compositional analysis, X-ray diffraction (XRD), Fourier-transform infrared spectroscopy (FTIR), transmission electron microscopy (TEM), and thermogravimetric analysis (TGA). This approach demonstrates a sustainable pathway for converting leaf waste into functional nanomaterials with potential applications in green composites, adsorption technologies, and beyond, while addressing the limitations of existing methods through a green and efficient methodology. This work is among the first to specifically valorize poplar leaf waste for the production of carboxylated cellulose nanocrystals. Its distinctive novelty stems from the integration of an underutilized, abundant agricultural residue with a sequential periodate-chlorite oxidation strategy. This approach provides a green alternative to conventional acid hydrolysis by operating under milder conditions and avoiding the use of harsh acids, thereby aligning with the principles of sustainable chemistry and waste-to-wealth conversion. The presented route not only addresses the limitations of existing feedstocks but also demonstrates a methodology tailored for introducing high surface functionality, positioning poplar leaves as a promising and novel resource for advanced nanomaterial synthesis.

2 Materials and Methods

2.1 Materials

The poplar leaves waste used in this study was supplied by Tangyuan Farm of Jiamusi University (Heilongjiang, China). The collected leaves were thoroughly cleaned to remove adhering dirt and cut into segments of 3–5 cm. These segments were then sun-dried for five days to achieve a water content below 10%. The dried material was subsequently ground into a powder (designated as PL) using a grinder. The compositional analysis of the dried poplar leaves was performed following the standard procedures established by the National Renewable Energy Laboratory (NREL). The measured contents of cellulose, hemicellulose, and lignin were 36%, 21%, and 22%, respectively. All chemicals, of analytical grade, were obtained from Guangdong Wengjiang Chemical Reagent Co., Ltd. (Guangdong, China) and used as received. Deionized water was employed in all experimental processes.

2.2 Methods

2.2.1 Isolation of Cellulose

The initial step involved an alkalization treatment to extract lignin and hemicellulose from the raw fibers. In this procedure, poplar leaf waste powder (PL) was immersed in a 5 wt% NaOH solution, maintained at 80°C for 120 min with continuous agitation, using a fiber-to-liquid ratio of 1:20 (w/v). Upon completion of the reaction, the mixture was allowed to cool to ambient temperature. The solid residue was then collected by filtration through a cloth filter, which retained the solids while allowing the dissolved lignin and hemicellulose to pass through. The collected solids were subsequently rinsed repeatedly with distilled water until a neutral pH was achieved, then dried in preparation for the subsequent stage [33].

A bleaching treatment was subsequently employed to eliminate any residual lignin, hemicellulose, and colored impurities, thereby yielding a whiter and purer cellulose product. The material from the previous step was subjected to heating at 80°C for 90 min in a solution containing 3% (v/v) H_2O_2 and 5% NaOH, under constant stirring. A fiber-to-solution ratio of 1:40 (w/v) was used for this process. After the reaction, the mixture was cooled and filtered with a cloth filter to isolate the purified cellulose. The resulting solid was thoroughly washed with distilled water to remove any residual chemicals, dried, and designated as PL-CEL for subsequent characterization and application.

2.2.2 Isolation of Cellulose Nanocrystals

Cellulose nanocrystals were isolated from the purified PL-CEL via periodate oxidation, adapting a previously established method. The oxidation conditions, including reagent ratios and reaction duration, were selected based on optimized protocols from literature to ensure efficient cleavage of C2–C3 bonds and subsequent carboxylation while preserving the crystalline structure of cellulose [34,35]. Typically, 4 g of cellulose was first soaked in deionized water for 24 h. Subsequently, 5.33 g of sodium periodate ($NaIO_4$) and 15.6 g of sodium chloride (NaCl) were introduced to the wet cellulose slurry, where NaCl was added to enhance the oxidation efficiency and reaction kinetics. The total volume of water was adjusted to 250 mL, inclusive of the moisture from the cellulose [36]. The oxidation was conducted at room temperature for 24 h under constant stirring. To maintain reaction integrity, the vessel was wrapped in multiple layers of aluminum foil to ensure a light-free environment. Upon completion, the reaction was quenched by adding 20 mL of ethylene glycol to consume any unreacted periodate. The resulting dialdehyde cellulose (DAC) was then collected and subjected to extensive washing using a centrifuge (TD5B, Changsha Yingtai Instrument Co., Ltd., China) at 3000× *g* for 5 min per cycle. This process was repeated with deionized water until the supernatant's conductivity fell below 30 μS/cm, ensuring the removal of ethylene glycol and formaldehyde by-products. The purified DAC was finally lyophilized using a vacuum freeze-dryer (FD-1A-50, Beijing Bo Yikang Experimental Instrument Co., Ltd., China).

For the subsequent conversion, one gram of the freeze-dried DAC was re-dispersed in 50 mL of water (accounting for its inherent moisture). To this suspension, 2.93 g of NaCl and a stoichiometric amount of sodium chlorite ($NaClO_2$) and hydrogen peroxide (H_2O_2), corresponding to twice the molar quantity of the aldehyde groups in the DAC were added. The reaction proceeded for 24 h at room temperature with continuous agitation, while the pH was maintained at 5.0 by the dropwise addition of 0.5 M NaOH [37]. The final product, dicarboxylic cellulose nanocrystals (DCNC, designated as PL-CNC), was precipitated by adding two volumes of ethanol (Fig. 2). The nanocrystals were then isolated by centrifugation (TG5B, Changsha Yingtai Instrument Co., Ltd., China) at 8500× *g* for 5 min and washed sequentially with 0.1 M NaOH (three times) and deionized water until the supernatant conductivity was again below 30 μS/cm.

The final PL-CNC product was stored at 4°C. The mass yield was calculated as the weight ratio of the obtained PL-CNCs to the initial mass of cellulose used in this step.

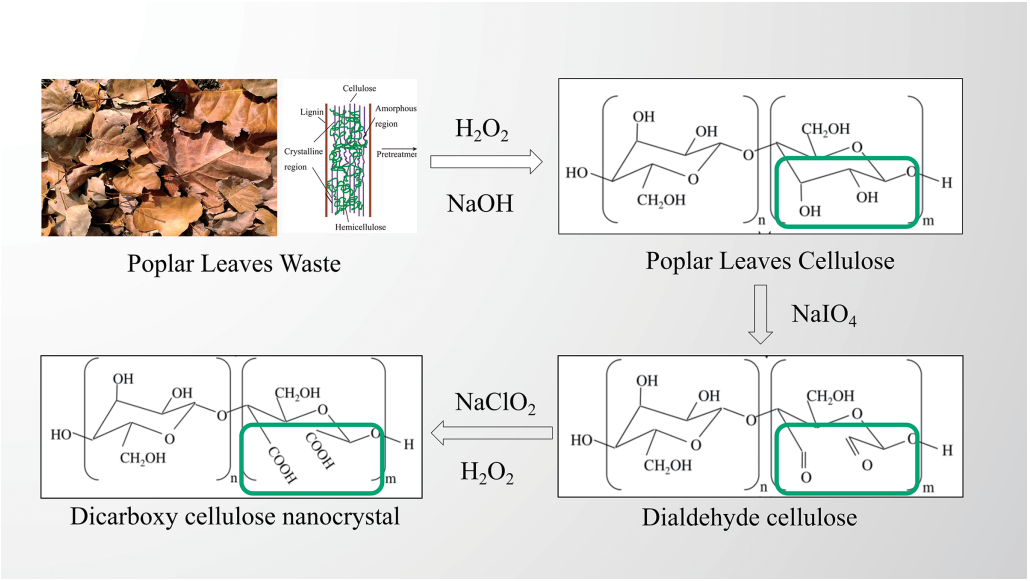

Figure 2: A chemical reaction scheme from poplar leaves waste to dicarboxy cellulose nanocrystal

2.3 Chemical Compositions

Compositional analyses of cellulose samples were performed with the ANKOM A200i semiautomatic fiber analyzer, which can determine the substance composition by measuring neutral detergent fiber (NDF), acid detergent fiber (ADF), and acid detergent lignin (ADL).

2.4 X-Ray Diffraction (XRD)

X-ray diffraction analysis was employed to investigate the structural evolution of the materials following each sequential treatment. The measurements were conducted on a Shimadzu XRD-700 Maxima X series diffractometer (Shimadzu Corp., Kyoto, Japan) operating with Cu Kα radiation (λ = 0.154 nm). Scans were performed over a 2θ range from 10° to 50° at a scanning rate of 2°/min, with the instrument configured at 40 kV and 30 mA. The crystallinity index (CrI) for each specimen was determined based on the Segal empirical method (Eq. (1)) [38]:

$$\mathrm{CrI}\ (\%) = \left[\left(I_{002} - I_{am}\right)/I_{002}\right]^{*}100\%, \tag{1}$$

in this equation, I_{002} signifies the maximum intensity of the (200) lattice diffraction peak, typically located at 2θ = 22.6°, which is attributed to the crystalline domains. I_{am} corresponds to the minimum intensity of the diffraction pattern in the amorphous region, observed at a 2θ angle of approximately 18°.

2.5 Fourier Transform Infrared (FTIR) Spectroscopy

Chemical structural analysis was performed using Fourier Transform Infrared (FTIR) spectroscopy. For each measurement, approximately 2 mg of a sample was homogenously blended with 150 mg of potassium bromide (KBr) of spectroscopic grade. The FTIR spectra were subsequently acquired on a Spectrum One spectrometer, collecting 64 scans per sample at a resolution of 4 cm^{-1}.

2.6 TEM Particle Size

The morphology of the cellulose nanocrystals (CNC) was examined using transmission electron microscopy (JEOL JEM-1400F, Tokyo, Japan). The analysis was performed at an accelerating voltage of 100 kV, with all experiments conducted in duplicate. Preparations involved depositing a droplet of a 1.0 wt% CNC suspension onto a copper grid, which was then air-dried at ambient temperature prior to imaging. Furthermore, the specific surface area of the nanocrystals was estimated based on a model that approximates their geometry as cylindrical rods, calculated using Eq. (2) [39]:

$$\text{Specific surface area}\left(\text{SSA}, \text{m}^2/\text{g}\right) = \frac{4}{\rho \cdot \text{d}}, \tag{2}$$

where ρ is the density of cellulose (1.5 g/cm^3) and d is the diameter of a single DCNC.

2.7 Conductometric Titration

The carboxyl content of the cellulose nanocrystals (CNCs) was quantified via conductometric titration. In a typical procedure, 0.1 g of CNC was dispersed in 100 mL of a 0.5 M NaCl aqueous solution under stirring. Subsequently, 5 mL of a mixed solution containing 0.1 M HCl and 0.5 M NaCl was introduced into the suspension. The titration was then carried out using a 0.1 M NaOH-0.5 M NaCl titrant under continuous agitation. An automatic potentiometric titrator (ZD-2, Shanghai LeiCi Magnetic Instrument Co., Ltd., China) recorded the potential changes throughout the process. Following the reaction, the data were processed according to a second-derivative method, where the volume of NaOH consumed was plotted against $\Delta E^2/\Delta V^2$. The inflection point on this curve indicated the total NaOH consumption, from which the volume specifically neutralized by carboxyl groups was determined. This entire procedure was repeated in triplicate. The carboxyl group content was calculated using Eq. (3) [40]:

$$C_{-\text{COOH}} = \frac{\left(V_{\text{NaOH}} - V_{\text{HCl}}\right) * M_{\text{NaOH}}}{W_{\text{cellulose}}}, \tag{3}$$

where $C_{-\text{COOH}}$ is the carboxyl content (mmol/g), V_{NaOH} is the volume of NaOH at the inflection point (mL), V_{HCl} is the volume of the 0.1 M HCl-0.5 M NaCl mixed solution added (mL), M_{NaOH} is the molar concentration of the NaOH solution (mol/L), and $W_{\text{cellulose}}$ is the mass of the CNCs used (g).

2.8 Thermogravimetric Analysis

The thermal decomposition behavior of the samples was investigated by thermogravimetric analysis (TGA) on a TGA 4000 instrument (PerkinElmer, Hopkinton, MA, USA). Each sample was loaded into an alumina crucible and heated from 50°C to 750°C at a constant rate of 10°C per minute under a nitrogen atmosphere with a flow rate of 20 mL/min. The resulting data on weight loss, derivative weight loss, and residual mass were processed and analyzed using Origin 2024 software.

2.9 Zeta Potential (ζ) Measurements

The colloidal stability of the cellulose nanocrystals was assessed by measuring their zeta potential (ζ). This analysis was performed using dynamic light scattering with phase analysis light scattering (PALS) mode on a Brookhaven Instruments analyzer. Sample suspensions (0.01 wt%) were prepared in double-distilled water, with the pH adjusted to 7.0 ± 0.2 using 0.1 M NaOH or HCl solutions, maintaining an ionic strength below 0.1 mM. Each suspension was allowed to equilibrate at 25°C for 10 min before measurement. All analyses were conducted in triplicate, and Smoluchowski's approximation was applied for the ζ potential calculation, consistent with the ISO 13099-2:2012 standard. To further examine the influence of ionic

strength, additional measurements were performed in NaCl solutions at concentrations ranging from 1 to 150 mM (pH 7.0).

2.10 Estimation of Molecular Weight

The apparent molecular weight ($M_{particle}$) of the PL-CNCs was estimated based on their geometric dimensions and density, following an established model for rod-like cellulose nanocrystals. This method calculates the mass of a single nanocrystal, approximating it as a perfect cylinder. First, the volume (V) of a single CNC particle was calculated using the formula for a cylinder: $V = \pi \times (D/2)^2 \times L$. Subsequently, the mass ($m_{particle}$) was determined using the density of crystalline cellulose ($\rho = 1.6$ g/cm^3): $m_{particle} = \rho \times V$. The number of glucose anhydride units (N) per particle was then derived using Avogadro's constant ($N_A = 6.022 \times 10^{23}$ mol^{-1}) and the molecular weight of a glucose anhydride unit ($M_{unit} = 162$ g/mol): $N = (m_{particle} \times N_A)/M_{unit}$. Finally, the apparent molecular weight was calculated as: $M_{particle} = N \times M_{unit}$.

3 Results and Discussion

3.1 Chemical Composition

The chemical composition of poplar leaves waste (PL) is pivotal in assessing its suitability as a feedstock for nanocellulose production. As summarized in Table 1, the raw PL contains 36% cellulose, 21% lignin, and 22% hemicellulose on a dry basis. This compositional profile situates PL favorably among commonly studied lignocellulosic residues [41,42]. Specifically, the cellulose content of PL (36%) is comparable to that of wheat straw (33%–40%) and rice straw (40%), and exceeds that of sugarcane bagasse (19%–24%) and walnut shell (27.4%). Although slightly lower than that of oil palm leaf (43.8%) and date leaves (39.9%), the cellulose content in PL remains sufficiently high to justify its valorization. More notably, the lignin content of PL (21%) is moderate-higher than that of rice straw (18%) and bean straw (9.35%), yet lower than that of walnut shell (36.31%) and sugarcane bagasse (25%–32%). This intermediate lignin level implies that a balanced pretreatment strategy can effectively remove lignin without excessive degradation of cellulose. The hemicellulose fraction (22%) is also within a typical range, similar to rice straw (20%–25%) but lower than oil palm leaf (36.4%) and date leaves (31.5%), which may facilitate easier extraction of cellulose with minimal hemicellulose interference.

The sequential alkalization and bleaching treatments were tailored to efficiently remove non-cellulosic components [43]. The alkalization step (5% NaOH, 80°C) disrupted the lignin-carbohydrate complex and solubilized a substantial portion of lignin and hemicellulose. Subsequent bleaching with alkaline hydrogen peroxide (3% H_2O_2/5% NaOH) further eliminated residual lignin and colored impurities, yielding a purified cellulose product (PL-CEL) with high whiteness and purity.

To quantitatively demonstrate the effectiveness of this purification, compositional analysis was performed on PL-CEL, revealing a cellulose content of 95.23%, hemicellulose of 1.35%, and lignin of 1.77%. This significant increase in cellulose purity (from 36% in raw PL to 95.23% in PL-CEL) confirms the robust removal of non-cellulosic components. The FTIR analysis (Section 3.3) further corroborates this, as the absence of characteristic peaks for lignin (e.g., 1595 cm^{-1} for aromatic C=C) and hemicellulose (e.g., 1242 cm^{-1} for C-O ester) in PL-CEL spectra aligns with the compositional data, providing strong evidence of successful purification. The effectiveness of these treatments is reflected in the high cellulose content of the resulting PL-CEL, confirming the robustness of the purification protocol in handling poplar leaves waste.

The mass yield of PL-CNCs, calculated as the weight ratio of the obtained nanocrystals to the initial mass of purified cellulose (PL-CEL), was 63.25%. This value demonstrates the efficiency of the

sequential periodate-chlorite oxidation in converting cellulose into functional nanocrystals with retained structural integrity. The suitability of PL for producing dicarboxylic cellulose nanocrystals (PL-CNC) is underscored not only by its cellulose content but also by its widespread availability and low cost as an agricultural waste. The moderate initial cellulose level is counterbalanced by the high process yield and the favorable physicochemical properties imparted by the subsequent periodate-chlorite oxidation. This oxidation pathway introduces a high density of carboxyl groups onto the cellulose surface, enhancing the hydrophilicity, colloidal stability, and potential for further functionalization of PL-CNC-attributes that are critically important for advanced material applications. Thus, the combination of satisfactory yield, abundant raw material supply, and mild processing conditions supports the economic viability and practical potential of poplar leaf waste as a sustainable feedstock for nanocellulose production, consistent with recent trends in agricultural waste valorization [44].

Table 1: Chemical composition of various cellulose samples (% dry matter)

Samples	Cellulose	Lignin	Hemicellulose	Ref.
Poplar leaves waste	36	21	22	This study
Poplar leaves purified cellulose	95.23	1.77	1.35	This study
Wheat straw	33–40	15–20	20–25	[45]
Rice straw	40	18	5.5	[46]
Date leaves	39.9	22.5	31.5	[47]
Walnut shell	27.4	36.31	31.3	[48]
Sugarcane bagasse	19–24	25–32	32–48	[49]
Oil palm leaf	43.8	19.07	36.4	[50]
Bean straw	30.64	9.35	23.14	[51]

3.2 X-Ray Diffraction

The X-ray diffraction patterns of the purified cellulose (PL-CEL) and the resulting dicarboxylic cellulose nanocrystals (PL-CNC) are presented in Fig. 3. Both samples display the characteristic diffraction peaks of cellulose I allomorph, with prominent reflections at approximately $2\theta = 15.2°$, $16.5°$ (collectively assigned to the (1–10) and (110) planes), and a strong peak at $2\theta = 22.6°$ corresponding to the (200) plane, which is indicative of the highly ordered crystalline structure [52,53]. The successful removal of amorphous components, primarily lignin and hemicellulose, through the sequential alkaline and bleaching treatments ($NaOH/H_2O_2$) is confirmed by the high crystallinity index (CrI) of 82% calculated for PL-CEL. This value is notably superior to that reported for many other biomass sources, such as Belulang grass (75.8%) and date palm waste (64.8%), underscoring the efficacy of the purification process applied to poplar leaves waste in isolating a highly crystalline cellulose fraction [47,54].

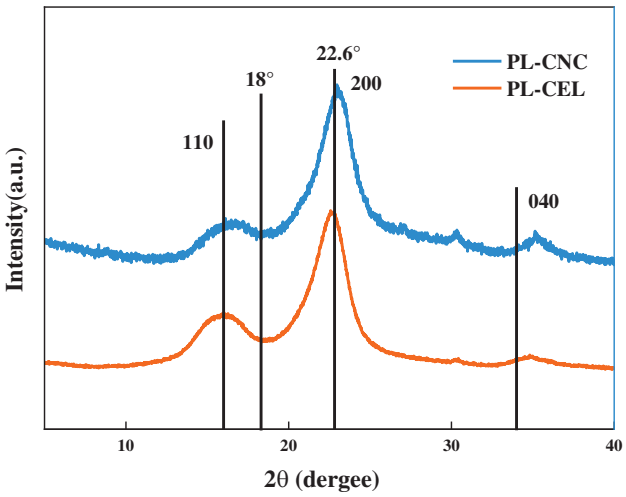

Figure 3: XRD patterns of purified cellulose (PL-CEL) and nanocellulose PL-CNC

Following the sequential periodate-chlorite oxidation, the CrI of the resulting PL-CNC decreased to 72.2% as summarized in Table 2. This reduction in crystallinity is a direct consequence of the chemical modifications imposed on the cellulose chains [55]. The periodate oxidation step selectively cleaves the C2–C3 bonds of the anhydroglucose units, converting the vicinal diols into dialdehyde groups. This reaction primarily occurs at the more accessible surfaces of the cellulose crystallites and within the disordered (amorphous) regions, disrupting the hydrogen-bonding network and consequently degrading the crystalline perfection [56]. Subsequent chlorite oxidation converts these aldehyde groups to carboxyl groups (-COOH), which introduce electrostatic repulsion and steric hindrance, further contributing to the partial disordering of the crystalline structure. The observed peak broadening in the PL-CNC pattern (particularly around the (200) reflection) corroborates this reduction in the average crystallite size and the introduction of structural defects.

Table 2: Chemical characteristics of PL-CNC

Sample	CrI (%)	Length (nm)	Width (nm)	Functional group content (-COOH, mmol/g)	Zeta potential (mV)	T_{max} (°C)
PL-CNC	72.2	271.22	14.68	1.9	−30.2	250

The crystallinity loss observed here (from 82% to 72.2%) aligns with the typical trend for chemically oxidized nanocellulones, where the introduction of surface functional groups often comes at the expense of crystalline integrity [57]. This contrasts with conventional acid hydrolysis (e.g., using H_2SO_4), which typically increases CrI by preferentially dissolving the amorphous regions. For instance, while acid hydrolysis of Belulang grass CNC increased CrI by nearly 24%, our oxidative route yielded a PL-CNC with a CrI (72.2%) that is lower than many conventional CNCs (often in the range of 78%–85%) but is consistent with, or even higher than, other dicarboxylated CNCs derived from sources like furfural residue (CrI ~11.4% post-oxidation) or sisal fibers (CrI ~62.2%) [58,59]. This comparison highlights the inherent trade-off between achieving high functional group content (carboxylation) and preserving crystallinity. The retained substantial crystallinity in PL-CNC (72.2%) indicates that the periodate-chlorite oxidation was effectively

controlled to introduce sufficient carboxyl groups for enhanced reactivity and dispersibility while largely preserving the rigid crystalline core, which is crucial for mechanical reinforcement in composite applications.

3.3 FTIR Analysis

Fourier transform infrared (FTIR) spectroscopy was employed to elucidate the chemical structural evolution of poplar leaves-derived cellulose throughout the sequential oxidation process. As illustrated in Fig. 4, the spectrum of purified cellulose (PL-CEL) exhibits characteristic bands of native cellulose I: a broad absorption at approximately 3340 cm^{-1} attributable to O–H stretching vibrations, along with signals at 2900 cm^{-1} (C–H stretching) and 1370 cm^{-1} (C–H bending), confirming the integrity of the cellulose backbone after alkali-bleaching pretreatment [60,61]. The absence of peaks associated with lignin (e.g., 1595 cm^{-1} for aromatic C=C) and hemicellulose (e.g., 1242 cm^{-1} for C–O ester) in PL-CEL validates the effectiveness of the purification protocol in removing non-cellulosic components, consistent with the compositional data presented in Table 1 [62].

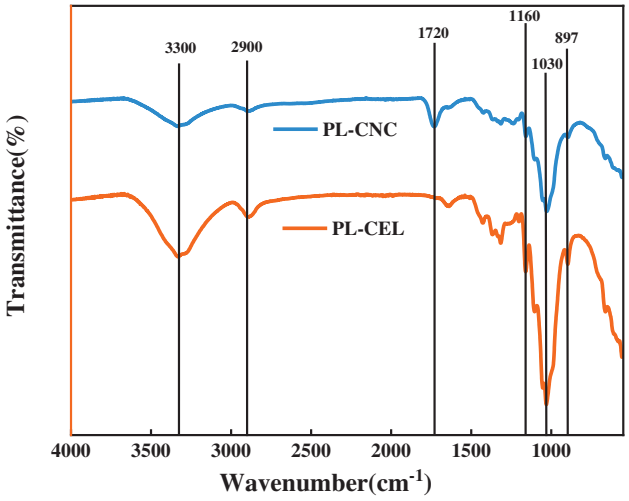

Figure 4: FTIR spectra recorded between 4000 and 500 cm^{-1} of purified cellulose (PL-CEL) and PL-CNC

Critical evidence for successful functionalization emerges in the spectrum of PL-CNC. A distinct and intense peak at 1720 cm^{-1} is observed, which is assigned to the C=O stretching vibration of carboxyl groups (–COOH) [63]. This signal is a direct consequence of the sequential periodate-chlorite oxidation: sodium periodate selectively cleaves the C2–C3 bonds of anhydroglucose units, generating dialdehyde cellulose intermediates with aldehyde functionalities. Subsequent oxidation using sodium chlorite converts these aldehyde groups to carboxyl groups via a haloform-like mechanism, as unequivocally confirmed by the pronounced intensity at 1720 cm^{-1} and the lack of residual aldehyde-specific absorptions near 875 cm^{-1} [64]. The concomitant appearance of a weak shoulder around 1600 cm^{-1} further suggests the presence of carboxylate anions ($–COO^-$), indicative of advanced decarboxylation [65].

The efficiency and practicality of the periodate-chlorite route are underscored by the high intensity of the 1720 cm^{-1} peak, which reflects a substantial degree of carboxyl group incorporation. This functionalization enhances the hydrophilicity and colloidal stability of PL-CNC, as corroborated by zeta potential measurements (Section 3.5). Moreover, the preservation of cellulose skeletal vibrations—such as the C–O–C glycosidic ether stretch at 1160 cm^{-1} and the pyranose ring vibration at 1055 cm^{-1}-indicates that oxidative modification primarily occurs at accessible amorphous regions and crystal surfaces, without extensive degradation of the crystalline core [66]. The retention of the β-glycosidic linkage band at 890 cm^{-1} further

supports the maintenance of structural integrity post-oxidation [67]. Thus, the FTIR results collectively affirm that the sequential oxidation strategy successfully introduces carboxyl groups while preserving the essential cellulose morphology, rendering PL-CNC highly suitable for advanced material applications.

3.4 Morphological and Functional Group Content Analysis

The morphological features of the dicarboxylic cellulose nanocrystals (PL-CNCs) extracted from poplar leaves waste were investigated using transmission electron microscopy (TEM). As depicted in Fig. 5a, the PL-CNCs exhibited a typical rod-like morphology with a homogeneous distribution, indicating successful disintegration of the cellulose fibers into nanoscale crystals. Statistical analysis of over 200 individual nanocrystals (Fig. 5b,c) revealed an average length of 271.22 ± 135.58 nm and an average width of 14.68 ± 8.44 nm. These dimensions are consistent with nanocellulose isolated from other agricultural residues such as rice straw (length: 297.7 nm, width: 13.3 nm) and wheat straw (length: 431.9 nm, width: 8.4 nm), confirming the effectiveness of the sequential periodate-chlorite oxidation in producing nanocellulose with comparable aspect ratios and nanoscale characteristics [55].

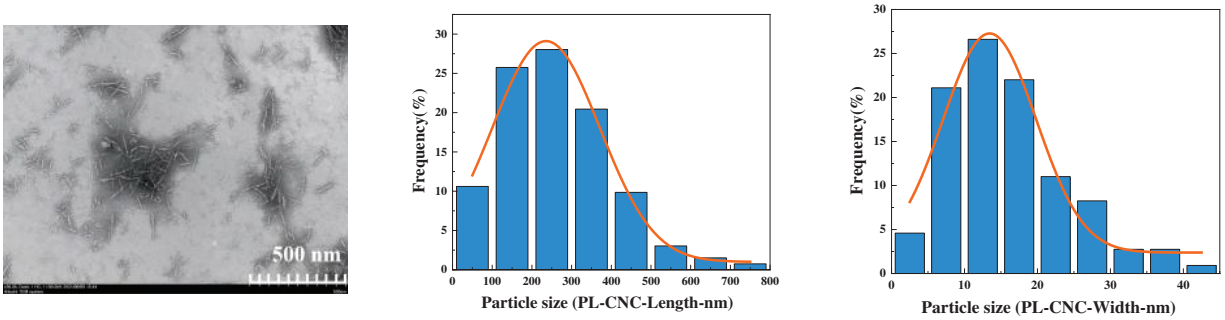

Figure 5: TEM image of PL-CNC (**a**), Particle size distribution curve of PL-CNC (**b**) Length, (**c**) Width

The high specific surface area (SSA) of PL-CNCs, calculated to be 276 m^2/g using the cylindrical model (Eq. (2)), underscores the successful nanofibrillation and exposure of reactive surfaces. This value is significantly higher than that of microcrystalline cellulose and is attributed to the efficient cleavage of amorphous regions and the introduction of surface carboxyl groups, which enhance hydrophilicity and dispersibility [35]. The substantial SSA is advantageous for applications requiring high interfacial interaction, such as adsorption, catalysis, and nanocomposite reinforcement [68].

The carboxyl group content of PL-CNCs, determined by conductometric titration, was 1.9 mmol/g. This high degree of functionalization is a direct result of the sequential oxidation process: sodium periodate selectively cleaves the C2–C3 bonds of the anhydroglucose units, converting vicinal diols into dialdehyde groups, which are subsequently oxidized by sodium chlorite to dicarboxylic groups [69]. The presence of carboxylate anions is further supported by the FTIR peak at 1720 cm^{-1} (Fig. 4), as also evidenced by the highly negative zeta potential (Section 3.5)—but also provides active sites for further chemical modification, such as grafting, crosslinking, or metal ion chelation [70].

Despite the overall good dispersion observed in TEM, some localized aggregation of nanocrystals was noted, which is common in nanocellulose samples due to strong interparticle hydrogen bonding and van der Waals forces. This phenomenon is exacerbated during drying processes, such as freeze-drying or air-drying, where ice crystal growth and capillary forces promote reassembly into larger aggregates [71]. Similar behavior

has been reported in nanocellulose derived from other lignocellulosic sources, including Helicters isora and spent edible fungus [57].

The combination of moderate crystallinity (72.2%, Section 3.2), high carboxyl content, and nanoscale dimensions positions PL-CNCs as a promising functional material for advanced applications such as water treatment, polymer composites, and biomedical systems [72,73]. The periodate-chlorite oxidation route offers a sustainable alternative to conventional acid hydrolysis, enabling tailored surface chemistry while maintaining structural integrity.

3.5 Zeta Potential

The zeta potential (ζ) of the dicarboxylic cellulose nanocrystals (PL-CNC) extracted from poplar leaves waste was measured to be −30.2 mV in neutral aqueous suspension (pH 7.0), indicating a moderately stable colloidal system. According to the classical DLVO theory, colloidal suspensions with $|\zeta| > 30$ mV are generally considered stable due to strong electrostatic repulsion between nanoparticles, which effectively counterbalances van der Waals attractive forces and prevents aggregation [74]. The observed ζ value of –30.2 mV lies at the threshold of high stability, which can be attributed to the high surface carboxyl group content (1.9 mmol/g) introduced by the sequential periodate-chlorite oxidation. These anionic carboxylate groups ($–COO^-$) impart a strong negative surface charge, enhancing the electrostatic repulsion among PL-CNC particles.

To further investigate the pH-dependent colloidal behavior, zeta potential measurements were conducted over a pH range of 3 to 10. Under acidic conditions (pH 3.0), the ζ potential increased to –12.5 mV due to protonation of carboxylate groups, which reduced the net surface charge and led to partial aggregation. In contrast, under alkaline conditions (pH 10.0), the ζ potential decreased to –38.7 mV, resulting from the deprotonation of surface functional groups and thus strengthening the electrostatic repulsion. Moreover, the influence of ionic strength on ζ potential was evaluated by adding NaCl (1–150 mM). At high ionic strength (150 mM NaCl, pH 7.0), the ζ potential dropped to –15.7 mV due to charge screening effects, which compressed the electrical double layer and reduced interparticle repulsion [75]. This sensitivity to ionic environment underscores the necessity of controlling salt concentration in processes such as nanocomposite preparation or aqueous coating formulations. The combination of high carboxyl content, nanoscale dimensions, and tunable surface charge makes PL-CNC a promising candidate for advanced applications including emulsion stabilization, polymer reinforcement, and environmental remediation. The results are consistent with previous studies on carboxylated nanocellulose, where similar ζ trends were reported for systems derived from wood pulp or agricultural residues [76,77].

3.6 Thermal Analysis

Thermogravimetric analysis (TGA) was conducted to evaluate the thermal stability and decomposition behavior of the purified cellulose (PL-CEL) and dicarboxylic cellulose nanocrystals (PL-CNC), as illustrated in Fig. 6. Both samples exhibited three main stages of mass loss, which are characteristic of cellulosic materials [78]. The initial stage, occurring between 50–150°C, corresponded to the evaporation of adsorbed water, with a mass loss of approximately 4%–6%, indicating the hygroscopic nature of the samples.

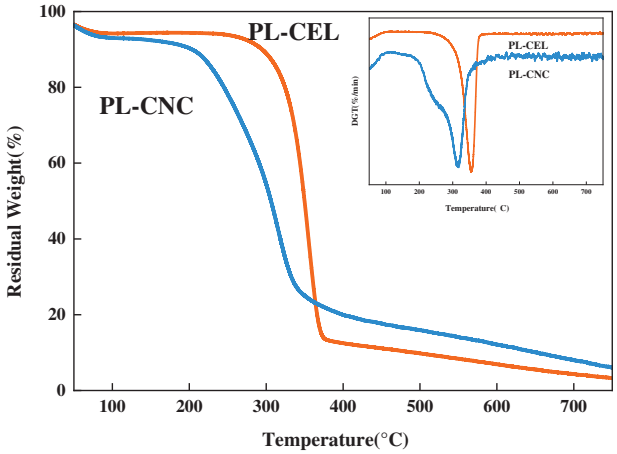

Figure 6: TGA curves of PL-CEL and PL-CNC

The second stage, spanning from approximately 220°C to 350°C, represented the primary thermal decomposition of cellulose. For PL-CEL, the maximum degradation rate occurred at around 330°C, which is typical for cellulose I and reflects the cleavage of glycosidic linkages, dehydration, and depolymerization reactions leading to the formation of volatile compounds such as levoglucosan, CO, CO_2, and H_2O [78,79]. In contrast, PL-CNC began to degrade at a lower onset temperature (~250°C), with a broader and less sharp degradation profile. This reduction in thermal stability can be attributed to the periodate-chlorite oxidation process, which introduces carboxyl groups and disrupts the hydrogen-bonding network within the cellulose crystalline structure [80]. The oxidative cleavage of C2–C3 bonds in the glucose units not only reduces molecular weight but also increases the accessibility of amorphous regions, facilitating earlier degradation [81].

The estimated apparent molecular weight of the PL-CNCs (approximately 2.84×10^6 g/mol) provides further insight into this thermal behavior. The sequential periodate-chlorite oxidation inevitably secludes cellulose chains within both amorphous and crystalline regions, leading to a reduction in the overall molecular weight and dimensions of the resulting nanocrystals compared to the native cellulose microfibrils. Materials with lower molecular weights typically exhibit lower thermal degradation temperatures because they possess a higher concentration of chain ends, which can initiate decomposition reactions, and a less stable, more disordered structure. The reduced molecular weight of PL-CNCs, consequent to the oxidative scission of glycosidic bonds, is therefore a contributing factor to their lower onset temperature of degradation compared to the higher molecular weight, more intact structure of PL-CEL.

The third stage, above 350°C up to 500°C, involved the further breakdown of carbonaceous residues and the formation of stable char [82]. Notably, PL-CNC exhibited a higher residual mass (~20%) compared to PL-CEL (~15%) at 500°C. This increased char yield suggests that the introduced carboxyl groups promote cross-linking and aromatization reactions at elevated temperatures, enhancing the thermal resistance of the nanocrystals under inert conditions. Such behavior aligns with previous studies on oxidized nanocellulones, where surface functionalization can lead to improved char formation despite lower initial degradation temperatures [83].

The observed thermal behavior underscores the trade-off between functionalization and structural integrity: while oxidation enhances surface reactivity and dispersibility, it modestly compromises the native thermal stability of cellulose. These findings are consistent with the structural modifications confirmed

by XRD and FTIR, and provide critical insight into the processing windows for potential applications of PL-CNC in materials requiring moderate thermal exposure.

4 Conclusions

This study successfully demonstrates the valorization of poplar leaf waste (PL) as a sustainable and promising feedstock for the production of carboxylated cellulose nanocrystals (PL-CNCs) via an integrated alkaline pretreatment and sequential periodate-chlorite oxidation route. The purified cellulose (PL-CEL) obtained after alkalization and bleaching exhibited high crystallinity (CrI = 82%) and purity, confirming the effectiveness of the pretreatment in removing non-cellulosic components. Subsequent oxidation yielded dicarboxylic cellulose nanocrystals (PL-CNCs) with a rod-like morphology (average length = 271 nm, width = 15 nm), high carboxyl group content (1.9 mmol/g), and a specific surface area of 276 m^2/g. The introduced carboxyl groups imparted excellent colloidal stability, as evidenced by a zeta potential of –30.2 mV at neutral pH. Although the oxidation process slightly reduced the crystallinity (CrI = 72.2%) and thermal stability compared to PL-CEL, the resulting PL-CNCs retained sufficient crystalline integrity and exhibited enhanced char formation at high temperatures. The combination of abundant raw material availability, mild chemical conditions, and tunable surface functionality positions this approach as a green and efficient alternative to conventional acid hydrolysis. The obtained PL-CNCs show great potential for advanced applications in nanocomposites, adsorption, and environmentally friendly materials, contributing to both agricultural waste management and sustainable nanomaterial production.

Acknowledgement: The authors would like to thank the College of Mechanical Engineering, Jiamusi University.

Funding Statement: This research was funded by the basic scientific research Funds project of Heilongjiang Universities, grant number 2023-KYYWF-0570.

Author Contributions: Dongwei Shao: Investigation, Data Curation, Writing—Original Draft, Visualization. Hao Sun: Methodology, Investigation. Qi Wang: Data Curation, Writing—Original Draft. Ping Han: Data Curation, Writing—Original Draft. Yiwei Liu: Writing—Original Draft, Visualization Jiyi Luan: Resources, Supervision. Lin Jia: Data Curation, Writing—Original Draft. Qiang He: Conceptualization, Writing—Original Draft, Supervision. Bo Cui: Conceptualization, Writing—Review & Editing, Supervision, Funding. All authors reviewed the results and approved the final version of the manuscript.

Availability of Data and Materials: Data available on request from the authors.

Ethics Approval: Not applicable.

Conflicts of Interest: The authors declare no conflicts of interest to report regarding the present study.

References

1. Sorieul M, Dickson A, Hill SJ, Pearson H. Plant fibre: molecular structure and biomechanical properties, of a complex living material, influencing its deconstruction towards a biobased composite. Materials. 2016;9(8):618. doi:10.3390/ma9080618.
2. Indran S, Raj RE. Characterization of new natural cellulosic fiber from *Cissus quadrangularis* stem. Carbohydr Polym. 2015;117:392–9. doi:10.1016/j.carbpol.2014.09.072.
3. Chen C, Hu L. Nanocellulose toward advanced energy storage devices: structure and electrochemistry. Acc Chem Res. 2018;51(12):3154–65. doi:10.1021/acs.accounts.8b00391.
4. Rana AK, Frollini E, Thakur VK. Cellulose nanocrystals: pretreatments, preparation strategies, and surface functionalization. Int J Biol Macromol. 2021;182:1554–81. doi:10.1016/j.ijbiomac.2021.05.119.

5. Loaiza JM, Gutiérrez EA, García JC, López F. Cascade biorefinery approach to obtain hemicelluloses, lignin, cellulose and nanocelluloses from high-yield forest crops (*Ulmus minor*) for different industrial applications. Ind Crops Prod. 2025;236(11):122031. doi:10.1016/j.indcrop.2025.122031.
6. Yang C, Duan G, Zhang C, Huang Y, Li S, Jiang S. Preparation and applications of magnetic nanocellulose composites: a review. Carbohydr Polym. 2025;354(8):123317. doi:10.1016/j.carbpol.2025.123317.
7. Ferreira FV, Souza AG, Ajdary R, de Souza LP, Lopes JH, Correa DS, et al. Nanocellulose-based porous materials: regulation and pathway to commercialization in regenerative medicine. Bioact Mater. 2023;29:151–76. doi:10.1016/j.bioactmat.2023.06.020.
8. Qi J, Zhang M, Xu T, Liu K, Wang Y, Zhang H, et al. Nanocellulose/metal-organic frameworks composites for advanced energy storage of electrodes and separators. Chem Eng J. 2024;500(4):157318. doi:10.1016/j.cej.2024.157318.
9. Wang C, Zhu L, Wang X, Tamer TM, Yao R, Rahman MM, et al. Application of nanocellulose in solar photo/thermal energy conversion and electrochemical energy storage devices. Green Carbon. 2025;3(3):225–45. doi:10.1016/j.greenca.2025.02.001.
10. Hou Y, Wu Z, Qin W, Loy DA, Lin D. A review on surface and interface engineering of nanocellulose and its application in smart packaging. Adv Colloid Interface Sci. 2025;345:103645. doi:10.1016/j.cis.2025.103645.
11. Sadat-Shojai M, Asadnia M, Zarei-fard N, Arvaneh AR. Electrospinning of liquefied banana stem residue in conjugation with hydroxyapatite nanocrystals: towards new scaffolds for bone tissue engineering. Cellulose. 2022;29(7):4039–56. doi:10.1007/s10570-022-04542-5.
12. Sun B, Zhang C, Li X, Zhong L, Zhang Z, Zhou D. Nanocellulose-based hydrogels for smart sensors. Carbohydr Polym. 2025;368(13):124152. doi:10.1016/j.carbpol.2025.124152.
13. Abd Rahman NMM, Olivito F, Selvam T, Al Qadr Imad Wan-Mohtar WA, Procopio A, Oza G, et al. Emerging cellulose applications in the era of ecological transition. Renew Sustain Energy Rev. 2026;226(10):116317. doi:10.1016/j.rser.2025.116317.
14. Xu YN, Tian D. Frontiers in cellulose@COFs composites: from multiform fabrication toward emerging applications in separation, environment, and energy. Coord Chem Rev. 2026;548:217143. doi:10.1016/j.ccr.2025.217143.
15. Chen L, Yu L, Qi L, Eichhorn SJ, Isogai A, Lizundia E, et al. Cellulose nanocomposites by supramolecular chemistry engineering. Nat Rev Mater. 2025;10(10):728–49. doi:10.1038/s41578-025-00810-5.
16. Asadnia M, Sadat-Shojai M. Recent perspective of synthesis and modification strategies of cellulose nanocrystals and cellulose nanofibrils and their beneficial impact in scaffold-based tissue engineering: a review. Int J Biol Macromol. 2025;293:139409. doi:10.1016/j.ijbiomac.2024.139409.
17. Wang X, Shen Z, Hao R, Zhang L, Li S, Xu X, et al. Nanocellulose prepared from shiitake mushroom (*Lentinus edodes*) stipe by high pressure homogenization and the gel-like emulsions stabilized by them. Int J Biol Macromol. 2025;300(32):140210. doi:10.1016/j.ijbiomac.2025.140210.
18. Hoo DY, Low ZL, Low DYS, Tang SY, Manickam S, Tan KW, et al. Ultrasonic cavitation: an effective cleaner and greener intensification technology in the extraction and surface modification of nanocellulose. Ultrason Sonochem. 2022;90:106176. doi:10.1016/j.ultsonch.2022.106176.
19. Hoseinpour Z, Niazmand R, Heydari-Majd M. Extraction and characterization of nanocellulose from *Cuminum cyminum* L. husk by ball-milling-assisted ultrasound. Carbohydr Polym Technol Appl. 2025;11(7):100934. doi:10.1016/j.carpta.2025.100934.
20. Cidreira ACM, Hatami T, Linan LZ, Pinheiro IF, Gomes RC, Rocha JJC, et al. Nanocellulose extraction from acai bagasse through mixed acid hydrolysis and oxidative techniques. Int J Biol Macromol. 2024;273:133034. doi:10.1016/j.ijbiomac.2024.133034.
21. Gunathilake TMSU, Ching YC, Uyama H, Nguyen DH, Chuah CH. Investigations on the interactions of proteins with nanocellulose produced via sulphuric acid hydrolysis. Int J Biol Macromol. 2021;193(10):1522–31. doi:10.1016/j.ijbiomac.2021.10.215.
22. Parsai G, Parikh PA, Parikh JK. Novel DES- ultrasonication assisted process for nanocellulose synthesis using Box Behnken design. Ind Crops Prod. 2024;217:118856. doi:10.1016/j.indcrop.2024.118856.

23. Wang S, Cheng X, Zhu E, Li T, Zhang L, Fan Y, et al. One-pot preparation of physical and chemical double-cross-linked nanocellulose/poly(deep eutectic solvent) conductive elastomers in acidic deep eutectic solvent (DES) system for 3D-printable information-storage expansion. Chem Eng J. 2024;488(50):151066. doi:10.1016/j.cej.2024.151066.
24. Wang S, Zhang L, Ali Khan K, Ullah MW, Fan Y, Wang Z. Deep eutectic solvents as a 'multifunctional operating platform' for nanocellulose production and modification: a review on sustainable composite advancements. Mater Sci Eng R Rep. 2025;165(5):101025. doi:10.1016/j.mser.2025.101025.
25. Madhushree M, Vairavel P, Mahesha GT, Bhat KS. Oxidative modifications of cellulose: methods, mechanisms, and emerging applications. J Nat Fibres. 2025;22(1):2497910. doi:10.1080/15440478.2025.2497910.
26. Qiu L, Li C, Zhang S, Wang S, Li B, Cui Z, et al. Distinct property of biochar from pyrolysis of poplar wood, bark, and leaves of the same origin. Ind Crops Prod. 2023;202(12):117001. doi:10.1016/j.indcrop.2023.117001.
27. Goren AY, Kenez M, Dincer I, Khalvati A. Cleaner production of biohydrogen using poplar leaves: experimental and optimization studies. J Clean Prod. 2024;434:140080. doi:10.1016/j.jclepro.2023.140080.
28. Alrasheedi NH. Sustainable microcrystalline cellulose extracted from biowaste *Tephrosia purpurea* leaves: biomass exfoliation and physicochemical characterisation. Biomass Convers Biorefin. 2025;15(9):13409–24. doi:10.1007/s13399-024-06009-y.
29. Sunesh NP, Senthamaraikannan P, Divakaran D, Benitha VS, Suyambulingam I, Vijay R, et al. Detailed analysis and characterisation of microcrystalline cellulose derived from *Ocimum tenuiflorum* leaves. Biomass Convers Biorefin. 2025;15(14):21573–88. doi:10.1007/s13399-025-06645-y.
30. Fouad H, Jawaid M, Karim Z, Meraj A, Abu-Jdayil B, Nasef MM, et al. Preparation and characterization of carboxymethyl microcrystalline cellulose from pineapple leaf fibre. Sci Rep. 2024;14(1):23286. doi:10.1038/s41598-024-73860-4.
31. Taye M, Chaudhary BU, Kale RD. Extraction and analysis of microcrystalline cellulose from delignified serte leaf fiber wastes. J Nat Fibres. 2021;18(11):1729–41. doi:10.1080/15440478.2019.1697992.
32. Rathinavelu R, Paramathma BS, Divkaran D, Siengchin S. Physicochemical, thermal, and morphological properties of microcrystalline cellulose extracted from *Calotropis gigantea* leaf. Biomass Convers Biorefin. 2024;14(19):24455–72. doi:10.1007/s13399-023-04370-y.
33. Harini K, Chandra Mohan C. Isolation and characterization of micro and nanocrystalline cellulose fibers from the walnut shell, corncob and sugarcane bagasse. Int J Biol Macromol. 2020;163:1375–83. doi:10.1016/j.ijbiomac.2020.07.239.
34. Sun X, Jiang F. Periodate oxidation-mediated nanocelluloses: preparation, functionalization, structural design, and applications. Carbohydr Polym. 2024;341(10):122305. doi:10.1016/j.carbpol.2024.122305.
35. Yang H, Alam MN, van de Ven TGM. Highly charged nanocrystalline cellulose and dicarboxylated cellulose from periodate and chlorite oxidized cellulose fibers. Cellulose. 2013;20(4):1865–75. doi:10.1007/s10570-013-9966-7.
36. Kou Z, Tolmachev D, Vuorte M, Sammalkorpi M. Interactions of NaCl with cellulose Iβcrystal surfaces and the effect on cellulose hydration: a molecular dynamics study. Cellulose. 2024;31(7):4115–29. doi:10.1007/s10570-024-05831-x.
37. Sun X, Xue Y, Li J, Yang Y, Bai Y, Chen Y. Fluorescent labeling and characterization of dicarboxylic cellulose nanocrystals prepared by sequential periodate-chlorite oxidation. RSC Adv. 2021;11(40):24694–701. doi:10.1039/d1ra04812k.
38. Segal L, Creely JJ, Martin AE Jr, Conrad CM. An empirical method for estimating the degree of crystallinity of native cellulose using the X-ray diffractometer. Text Res J. 1959;29(10):786–94. doi:10.1177/004051755902901003.
39. Serra A, González I, Oliver-Ortega H, Tarrès Q, Delgado-Aguilar M, Mutjé P. Reducing the amount of catalyst in TEMPO-oxidized cellulose nanofibers: effect on properties and cost. Polymers. 2017;9(11):557. doi:10.3390/polym9110557.
40. Araki J, Wada M, Kuga S. Steric stabilization of a cellulose microcrystal suspension by poly(ethylene glycol) grafting. Langmuir. 2001;17(1):21–7. doi:10.1021/la001070m.

41. Velmurugan T, Suganya Priyadharshini G, Suyambulingam I, Siengchin S. Extraction and characterization of *Thespesia populnea* leaf cellulose: a biomass to biomaterial conversion. Biomass Convers Biorefin. 2024;14(23):30833–44. doi:10.1007/s13399-024-06018-x.
42. JIA S, Yang XH, Ni PY, Yun JL. Magnetic hydrogels from Apocynum leaf cellulose and chitosan: synthesis, characterization, and adsorption performance study. Iran Polym J. 2025; 1–20. doi:10.1007/s13726-025-01553-4.
43. Kamali Moghaddam M, Torabi T. Cellulose microfibers isolated from *Yucca* leaves: structural, chemical, and thermal properties. J Nat Fibres. 2022;19(16):13120–30. doi:10.1080/15440478.2022.2085229.
44. Xue H, Zhang Y, Zhao Z, Gao H, Bao W, Li J, et al. A review: sources, preparation and application of nanocellulose. J Polym Mater. 2025;42(2):379–409. doi:10.32604/jpm.2025.066695.
45. Kaushik A, Singh M, Verma G. Green nanocomposites based on thermoplastic starch and steam exploded cellulose nanofibrils from wheat straw. Carbohydr Polym. 2010;82(2):337–45. doi:10.1016/j.carbpol.2010.04.063.
46. Lu P, Hsieh YL. Preparation and characterization of cellulose nanocrystals from rice straw. Carbohydr Polym. 2012;87(1):564–73. doi:10.1016/j.carbpol.2011.08.022.
47. Mostafa H, Airouyuwaa JO, Hamed F, Wang Y, Maqsood S. Structural, mechanical, antioxidant and antibacterial properties of soy protein isolate (SPI)-based edible food packaging films as influenced by nanocellulose (NC) and green extracted phenolic compounds from date palm leaves. Food Packag Shelf Life. 2023;38(1):101124. doi:10.1016/j.fpsl.2023.101124.
48. Orue A, Eceiza A, Arbelaiz A. The use of alkali treated walnut shells as filler in plasticized poly(lactic acid) matrix composites. Ind Crops Prod. 2020;145:111993. doi:10.1016/j.indcrop.2019.111993.
49. Gabriel T, Belete A, Syrowatka F, Neubert RHH, Gebre-Mariam T. Extraction and characterization of celluloses from various plant byproducts. Int J Biol Macromol. 2020;158:1248–58. doi:10.1016/j.ijbiomac.2020.04.264.
50. Kumneadklang S, Larpkiattaworn S, Niyasom C, O-Thong S. Bioethanol production from oil palm frond by simultaneous saccharification and fermentation. Energy Proc. 2015;79:784–90. doi:10.1016/j.egypro.2015.11.567.
51. Petersson A, Thomsen MH, Hauggaard-Nielsen H, Thomsen AB. Potential bioethanol and biogas production using lignocellulosic biomass from winter rye, oilseed rape and faba bean. Biomass Bioenergy. 2007;31(11–12):812–9. doi:10.1016/j.biombioe.2007.06.001.
52. Browne C, Raghuwanshi VS, Lin M, Garnier G, Batchelor W. Characterisation of cellulose nanocrystals by rheology and small angle X-ray scattering (SAXS). Colloids Surf A Physicochem Eng Aspects. 2022;651(7):129532. doi:10.1016/j.colsurfa.2022.129532.
53. Beroual M, Trache D, Mehelli O, Boumaza L, Tarchoun AF, Derradji M, et al. Effect of the delignification process on the physicochemical properties and thermal stability of microcrystalline cellulose extracted from date palm fronds. Waste Biomass Valorization. 2021;12(5):2779–93. doi:10.1007/s12649-020-01198-9.
54. Pratama AW, Mahardika M, Widiastuti N, Piluharto B, Ilyas RA, Sapuan SM, et al. Isolation and characterization of highly thermal stable microcrystalline cellulose derived from belulang grass (*Eleusine indica*). Case Stud Chem Environ Eng. 2024;9:100743. doi:10.1016/j.cscee.2024.100743.
55. Sun X, He Q, Yang Y. Preparation of dicarboxyl cellulose nanocrystals from agricultural wastes by Sequential periodate-chlorite oxidation. J Renew Mater. 2020;8(4):447–60. doi:10.32604/jrm.2020.09671.
56. Yang H, Chen D, van de Ven TGM. Preparation and characterization of sterically stabilized nanocrystalline cellulose obtained by periodate oxidation of cellulose fibers. Cellulose. 2015;22(3):1743–52. doi:10.1007/s10570-015-0584-4.
57. He Q, Yang Y, Liu Z, Shao D, Jiang D, Xing L, et al. Preparation and characterization of cellulose nanocrystals from spent edible fungus substrate. J Sci Food Agric. 2022;102(7):2761–72. doi:10.1002/jsfa.11617.
58. Liu L, Li Q, Wan C. Deep eutectic solvent-based microextraction system for simultaneous lignocellulose fractionation and furfural production. Green Chem. 2025;27(5):1519–28. doi:10.1039/d4gc02874k.
59. Fan F, Zhu M, Fang K, Cao E, Yang Y, Xie J, et al. Extraction and characterization of cellulose nanowhiskers from TEMPO oxidized sisal fibers. Cellulose. 2022;29(1):213–22. doi:10.1007/s10570-021-04305-8.
60. Hafid HS, Omar FN, Zhu J, Wakisaka M. Enhanced crystallinity and thermal properties of cellulose from rice husk using acid hydrolysis treatment. Carbohydr Polym. 2021;260:117789. doi:10.1016/j.carbpol.2021.117789.

61. Baruah J, Bardhan P, Mukherjee AK, Deka RC, Mandal M, Kalita E. Integrated pretreatment of banana agrowastes: structural characterization and enhancement of enzymatic hydrolysis of cellulose obtained from banana peduncle. Int J Biol Macromol. 2022;201(1):298–307. doi:10.1016/j.ijbiomac.2021.12.179.
62. Hamdan MA, Ramli NA, Othman NA, Mohd Amin KN, Adam F. Characterization and property investigation of microcrystalline cellulose (MCC) and carboxymethyl cellulose (CMC) filler on the carrageenan-based biocomposite film. Mater Today Proc. 2021;42(2):56–62. doi:10.1016/j.matpr.2020.09.304.
63. Sun R, Tomkinson J. Separation and characterization of cellulose from wheat straw. Sep Sci Technol. 2005;39(2):391–411. doi:10.1081/SS-120027565.
64. Sun XF, Sun RC, Fowler P, Baird MS. Isolation and characterisation of cellulose obtained by a two-stage treatment with organosolv and cyanamide activated hydrogen peroxide from wheat straw. Carbohydr Polym. 2004;55(4):379–91. doi:10.1016/j.carbpol.2003.10.004.
65. Ilyas RA, Sapuan SM, Ibrahim R, Abral H, Ishak MR, Zainudin ES, et al. Sugar palm (*Arenga pinnate* (*Wurmb*.) *Merr*) cellulosic fibre hierarchy: a comprehensive approach from macro to nano scale. J Mater Res Technol. 2019;8(3):2753–66. doi:10.1016/j.jmrt.2019.04.011.
66. He Q, Bai Y, Lu Y, Cui B, Huang Z, Yang Q, et al. Isolation and characterization of cellulose nanocrystals from Chinese medicine residues. Biomass Convers Biorefin. 2024;14(21):27745–54. doi:10.1007/s13399-022-03380-6.
67. Yu Y, Guo W, Qu J, Wang S, Wang X, He Y, et al. Preparation and characterization of dialdehyde cellulose nanocrystals from the waste nutshell. Environ Dev Sustain. 2025;27(5):10789–805. doi:10.1007/s10668-023-04332-4.
68. Huber T, Graupner N, Müssig J. Regenerated cellulose fibres and their composites: from fundamental properties to advanced applications. Prog Mater Sci. 2026;156(3):101547. doi:10.1016/j.pmatsci.2025.101547.
69. Chen D, van de Ven TGM. Morphological changes of sterically stabilized nanocrystalline cellulose after periodate oxidation. Cellulose. 2016;23(2):1051–9. doi:10.1007/s10570-016-0862-9.
70. Fan XM, Yu HY, Wang DC, Mao ZH, Yao J, Tam KC. Facile and green synthesis of carboxylated cellulose nanocrystals as efficient adsorbents in wastewater treatments. ACS Sustainable Chem Eng. 2019;7(21):18067–75. doi:10.1021/acssuschemeng.9b05081.
71. He Q, Sun X, Bai Y, Meng X, Li C. Isolation of dicarboxy cellulose nanocrystal from spent fungi substrate and redispersion with gelatin. J Mol Liq. 2022;367(8):120397. doi:10.1016/j.molliq.2022.120397.
72. Tran GT, Nguyen TTT, Nguyen DTC, Van Tran T. Bacterial cellulose and composites for the treatment of water pollution: a review. Environ Chem Lett. 2025;23(2):707–32. doi:10.1007/s10311-025-01818-7.
73. Won T, Goh M, Lim C, Moon J, Lee K, Park J, et al. Recent progress in cellulose nanofibril hydrogels for biomedical applications. Polymers. 2025;17(17):2272. doi:10.3390/polym17172272.
74. Netzer F, Manian AP, Bechtold T, Pham T. The role of carboxyl and cationic groups in low-level cationised cellulose fibres investigated by *Zeta* potential and sorption studies. Cellulose. 2024;31(14):8501–17. doi:10.1007/s10570-024-06132-z.
75. Anikushin BM, Lagutin PG, Kanbetova AM, Novikov AA, Vinokurov VA. *Zeta* Potential of nanosized particles of cellulose as a function of pH. Chem Technol Fuels Oils. 2022;57(6):913–6. doi:10.1007/s10553-022-01328-0.
76. Adeniyi A, Gonzalez-Ortiz D, Pochat-Bohatier C, Mbakop S, Onyango MS. A comparison of unmodified and sawdust derived-cellulose nanocrystals (CNC)-modified polyamide membrane using X-ray photoelectron spectroscopy and *Zeta* Potential analysis. Polymers. 2023;15(1):57. doi:10.3390/polym15010057.
77. Xue W, Lei F, Li P, Jiang J. Cellulose accessibility and *Zeta* potentials of sugarcane bagasse pretreated by green liquor and ethanol for high hydrolysis efficiency. BioResources. 2017;13(1):1510–24. doi:10.15376/biores.13.1.1510-1524.
78. Debiagi P, Piazza V, Papagni M, Beretta A, Frassoldati A, Faravelli T. Cellulose pyrolysis kinetic model: detailed description of volatile species. Proc Combust Inst. 2024;40(1–4):105651. doi:10.1016/j.proci.2024.105651.
79. Chen J, Lu Z, Cai J, Lin Y, Li Y, Yao S. Investigation of primary and secondary char formation during pyrolysis of torrefied cellulose. J Anal Appl Pyrolysis. 2025;191:107187. doi:10.1016/j.jaap.2025.107187.
80. Zhang S, Feng J, Feng J, Jiang Y, Ding F. Carbon aerogels by pyrolysis of TEMPO-oxidized cellulose. Appl Surf Sci. 2018;440(19):873–9. doi:10.1016/j.apsusc.2018.01.252.

81. Leng E, Zhang Y, Peng Y, Gong X, Mao M, Li X, et al. *In situ* structural changes of crystalline and amorphous cellulose during slow pyrolysis at low temperatures. Fuel. 2018;216(1):313–21. doi:10.1016/j.fuel.2017.11.083.
82. Li X, Cen K, Wang L, Jia D, Zhu X, Chen D. Co-pyrolysis of cellulose and lignin: effects of pyrolysis temperature, residence time, and lignin percentage on the properties of biochar using response surface methodology. Ind Crops Prod. 2024;219:119071. doi:10.1016/j.indcrop.2024.119071.
83. Odak K, Warren KJ, Smith NA, Weimer AW. A phenomenological model for cellulose charring during low temperature pyrolysis. J Anal Appl Pyrolysis. 2025;192(8):107330. doi:10.1016/j.jaap.2025.107330.